The 3D Nonlinear Dynamics of Catenary Slender Structures for Marine Applications

Ioannis K. Chatjigeorgiou and Spyros A. Mavrakos
National Technical University of Athens
Greece

1. Introduction

Riser systems are inextricable parts of integrated floating production and offloading systems as they are used to convey oil from the seafloor to the offshore unit. Risers are installed vertically or they are laid obtaining a catenary configuration. From the theoretical point of view they can be formulated as slender structures obeying to the principles of the Euler-Bernoulli beams. Riser-type catenary slender structures and especially Steel Catenary Risers (SCRs) attract the attention of industry for many years as they are very promising for deep water applications. According to the Committee V.5 of the International Ship and Offshore Structures Congress (ISSC, 2003), "flexible risers have been qualified to 1500m and are expected to be installed in depths up to 3000m in the next few years". In such huge depths where the suspended length of the catenary will unavoidably count several kilometers, the equivalent elastic stiffness of the structure will be quite low enabling large displacements. The later remark implies that even small excitations could cause significant excursions in both in-plane and out-of-plane directions. Therefore a 2D formulation, although adequate in predicting the associated dynamics in the reference plane of the static equilibrium, it would be certainly a short approximation.

Furthermore, in deep water installations, for practical reasons mainly, the riser should be configured nearly as a vertical structure in order to avoid suspending more material. The nearly vertical configuration which ends in a sharp increase of the curvature close to the bottom, results in extreme bending moments at the touch down region. The static bending moment which is applied in the plane of reference of the catenary is further amplified due to the imposed excitation set by the motions of the floating structure. It has been generally acknowledged that the heave motion is the worst loading condition as it causes several effects, which depending on the properties of the excitation, can be applied individually or in combination between each other. Indicative examples are the seafloor interaction, buckling-like effects, "compression loading" and heave induced out-of-plane motions.

For the formulation of the seafloor interaction, various approaches have been proposed and it appears that the associated effects continue to attract the attention of the research community (Leira et al., 2004; Aubeny et al., 2006; Pesce et al., 2006; Clukey et al., 2008). "Compression loading" has been studied mainly in 2D (Passano & Larsen, 2006 & 2007; Chatjigeorgiou et al., 2007; Chatjigeorgiou, 2008), while buckling-like effects and possible

Source: Nonlinear Dynamics, Book edited by: Todd Evans,
ISBN 978-953-7619-61-9, pp. 366, January 2010, INTECH, Croatia, downloaded from SCIYO.COM

destabilizations are mainly considered for completely vertical structures (Kuiper & Mertikine, 2005; Gadagi & Benaroya, 2006; Chandrasekaran et al., 2006; Kuiper et al., 2008).

The content of the present work falls in the last category of the effects that were mentioned previously. The main concern of the study is to identify the details of the out-of-plane response which is induced due to motions imposed in the catenary's plane of reference and in particular due to heave excitation. Relevant effects called as "Heave Induced Motions" have been investigated experimentally in the past by Joint Industry Projects (JIP). According to HILM (Heave Induced Lateral Motions of Steel Catenary Risers) JIP led by Institut français du pétrole (Ifp), the phenomenon was first recorded during the HCR (Highly Compliant Riser Large Scale Model Tests) JIP led by PMB Engineering, in which a steel catenary riser was excited by heave motion in a stillwater lake. The pipe was subjected to out-of-plane cyclic motions. The same behaviour was observed during the HILM JIP measurements (LeCunff et al., 2005).

Apparently, the associated phenomena can be captured numerically only by treating the governing 3D dynamical system. To this end, the associated system is properly elaborated and solved numerically using an efficient finite differences numerical scheme.

2. Definitions

A fully immersed catenary slender structure is considered. The catenary is modeled as an Euler-Bernoulli slender beam, having the following geometrical and physical properties: suspended length L, outer diameter d_o, inner diameter d_i, submerged weight w_o, mass m, hydrodynamic mass m_a, cross sectional area A and moment of inertia I. The quantities d_o, d_i, A and I, correspond to the unstretched condition, while w_o, m and m_a are defined per unit unstretched length. The Young modulus of elasticity is denoted by E and accordingly EA and EI define the elastic and bending stiffness respectively. Finally, it is assumed that the catenary conforms to a linear stress-strain relation.

Next the generalized motion and loading vectors (Fig. 1) are defined. These are

$$\vec{V}(s;t) = \begin{bmatrix} u & v & w & \phi & \theta \end{bmatrix}^T \tag{1}$$

$$\vec{F}(s;t) = \begin{bmatrix} T & S_n & S_b & M_b & M_n \end{bmatrix}^T \tag{2}$$

where u, v, w are the tangential (axial), normal and bi-normal velocities, respectively, ϕ is the Eulerian angle which is formed between the tangent of the line and the horizontal in the reference plane of the catenary, θ is the Eulerian angle in the out-of-plane direction, T is the tension, S_n and S_b are the in-plane and the out-of-plane shear forces and finally M_b and M_n are the bending moments around the corresponding Lagrangian axes $\vec{b}$ and $\vec{n}$, namely the generalized loading that causes bending in the in-plane and the out-of-plane direction, respectively. The moments M_b and M_n are associated with the corresponding curvatures Ω_b and Ω_n according to $M_j=EI\Omega_j$, for $j=n,b$.

In the general case where steady current is presented, the relative velocities should be considered. These are written as $v_{tr} = u - U_t$, $v_{nr} = v - U_n$ and $v_{br} = w - U_b$, where U_t, U_n and U_b are the components of the steady current parallel to $\vec{t}$, $\vec{n}$ and $\vec{b}$, respectively. The elements of the vectors defined through Eqs. (1) and (2) are all functions of time t and the unstretched Lagrangian coordinate s.

3. Dynamic system

The 3D dynamic equilibrium of the submerged catenary is governed by ten partial differential equations. These equations are provided in the following without further details on the derivation procedure. For more details the reader is referenced to the works of Howell (1992), Burgess (1993), Triantafyllou (1994) and Tjavaras et al. (1998).

$$m\left(\frac{\partial u}{\partial t}+w\frac{\partial \theta}{\partial t}-v\frac{\partial \phi}{\partial t}\cos\theta\right)=\frac{\partial T}{\partial s}+S_b\Omega_n-S_n\Omega_b-w_0\sin\phi\cos\theta+R_{dt} \tag{3}$$

$$m\left(\frac{\partial v}{\partial t}+\frac{\partial \phi}{\partial t}\left(u\cos\theta+w\sin\theta\right)\right)+m_a\frac{\partial v_{nr}}{\partial t}=\frac{\partial S_n}{\partial s}+\Omega_b\left(T+S_b\tan\theta\right)-w_0\cos\phi+R_{dn} \tag{4}$$

$$m\left(\frac{\partial w}{\partial t}-v\frac{\partial \phi}{\partial t}\sin\theta-u\frac{\partial \theta}{\partial t}\right)+m_a\frac{\partial v_{br}}{\partial t}=\frac{\partial S_b}{\partial s}-S_n\Omega_b\tan\theta-T\Omega_n-w_0\sin\phi\sin\theta+R_{db} \tag{5}$$

$$\frac{1}{EA}\frac{\partial T}{\partial t}=\frac{\partial u}{\partial s}+\Omega_n w-\Omega_b v \tag{6}$$

$$\left(1+\frac{T}{EA}\right)\frac{\partial \phi}{\partial t}\cos\theta=\frac{\partial v}{\partial s}+\Omega_b\left(u+w\tan\theta\right) \tag{7}$$

$$-\left(1+\frac{T}{EA}\right)\frac{\partial \theta}{\partial t}=\frac{\partial w}{\partial s}-\Omega_b v\tan\theta-\Omega_n u \tag{8}$$

$$EI\frac{\partial \Omega_n}{\partial s}=EI\Omega_b^2\tan\theta+S_b\left(1+\frac{T}{EA}\right)^3 \tag{9}$$

$$EI\frac{\partial \Omega_b}{\partial s}=EI\Omega_n\Omega_b\tan\theta-S_b\left(1+\frac{T}{EA}\right)^3 \tag{10}$$

$$\frac{\partial \theta}{\partial s}=\Omega_n \tag{11}$$

$$\frac{\partial \phi}{\partial s}\cos\theta=\Omega_b \tag{12}$$

In Eqs. (3)-(5) R_{dt}, R_{dn} and R_{db} denote the nonlinear drag forces which are expressed using the Morison's formula. Thus,

$$R_{dt}=-\frac{1}{2}\pi\rho d_o C_{dt}v_{tr}\left|v_{tr}\right|(1+e)^{1/2} \tag{13}$$

$$R_{dn}=-\frac{1}{2}\rho d_o C_{dn}v_{nr}\left|v_{nr}^2+v_{br}^2\right|^{1/2}(1+e)^{1/2} \tag{14}$$

$$R_{db} = -\frac{1}{2}\rho d_o C_{db} v_{br} \left| v_{nr}^2 + v_{br}^2 \right|^{1/2} (1+e)^{1/2} \tag{15}$$

where C_{dt}, C_{dn} and C_{db} are the drag coefficients in tangential, normal and bi-normal directions respectively. Normally, for a cylindrical structure, the in-plane and the out-of-plane drag coefficients are equal while the tangential coefficient is very small and the associated term can be ignored without loss of accuracy. Finally, e denotes the axial strain deformation, which for a linear stress-strain relation is written as $e=T/EA$.

4. Numerical solution of the governing system using finite differences

The numerical method employed herein, is the finite differences box approximation (Hoffman, 1993). Unlike the very popular finite element methods, the existing works which are related to the application of numerical approximations that rely on finite differences, concern mainly the dynamics of cables and mooring lines which have a negligible bending stiffness (Burgess, 1993; Tjavaras et al., 1998; Ablow & Schechter, 1983; Howell, 1991; Chatjigeorgiou & Mavrakos, 1999 & 2000; Gobat & Grosenbaugh, 2001 & 2006; Gobat et al., 2002). The employment of the bending stiffness in mathematical formulations of cable dynamics is done for special applications such as low tension cables, towing cables, highly extensible cables and mooring lines in which the cycling loading leads to slacking conditions, i.e. cancellation of the total tension.

With regard to the studies on pipes, for which the omission of the bending stiffness will unavoidably lead to loss of important information, the finite differences approximation has been used mainly for the solution of the static equilibrium problem (Zare & Datta, 1988; Jain 1994) or as a numerical scheme for the integration in the time domain, alternative to Houbolt, Wilson-θ and Newmark-β methods (Patel & Seyed, 1995). As far as the dynamic equilibrium problem is concerned, box approximation has been employed recently by Chatjigeorgiou (2008) for the development of a solution tool that treats the two dimensional nonlinear dynamics of marine catenary risers.

For the governing system at hand (Eqs. (3)-(12)), the recommended procedure for employing a finite differences approximation requires that the set of equations should be first cast in a matrix-vector form. Thus, the concerned equations are written as

$$\mathbf{M}\frac{\partial \mathbf{Y}}{\partial t} + \mathbf{K}\frac{\partial \mathbf{Y}}{\partial s} + \mathbf{F}(\mathbf{Y}_{,s,t}) = 0 \tag{16}$$

where $\mathbf{Y} = [u \quad v \quad w \quad T \quad \phi \quad \theta \quad S_b \quad S_n \quad \Omega_n \quad \Omega_b]^{\mathbf{T}}$. The mass and stiffness matrices, **M** and **K**, and the forcing vector **F** are defined in Appendix A.

Next, Eq. (16) is discretized in both time and space using the finite differences box approximation. This is the approach taken by several authors mentioned in the references section of the present work. With this scheme, the discrete equations are written using what look like traditional backward differences, but because the discetization is applied on the half-grid points the method is second-order accurate. The result is a four point average, centered around the half-grid point. Thus, Eq. (16) becomes

$$\left(\mathrm{M}_k^{i+1} + \mathrm{M}_k^i\right)\left(\frac{\mathrm{Y}_k^{i+1} - \mathrm{Y}_k^i}{\Delta t}\right) + \left(\mathrm{M}_{k-1}^{i+1} + \mathrm{M}_{k-1}^i\right)\left(\frac{\mathrm{Y}_{k-1}^{i+1} - \mathrm{Y}_{k-1}^i}{\Delta t}\right)$$

$$+\left(\mathrm{K}_{k-1}^{i+1}+\mathrm{K}_{k}^{i+1}\right)\left(\frac{\mathrm{Y}_{k}^{i+1}-\mathrm{Y}_{k-1}^{i+1}}{\Delta s}\right)+\left(\mathrm{K}_{k-1}^{i}+\mathrm{K}_{k}^{i}\right)\left(\frac{\mathrm{Y}_{k}^{i}-\mathrm{Y}_{k-1}^{i}}{\Delta s}\right)$$
$$+\left(\mathrm{F}_{k}^{i+1}+\mathrm{F}_{k-1}^{i+1}+\mathrm{F}_{k}^{i}+\mathrm{F}_{k-1}^{i}\right)=0 \tag{17}$$

According to the matrix-vector Eq. (17) the governing partial differential equations are defined in the center of $[i,i+1]$ and $[k-1,k]$, namely at $[i+1/2, k-1/2]$. The subscripts k define the spatial grid points (the nodes) and the superscripts i define the temporal grid points (the time steps). For n nodal points (k=1 corresponds to the touch down point at s=0 and k=n corresponds to the top terminal point where the excitation is applied) Eq. (17) defines a system of $10\cdot(n-1)$ equations to be solved for the $10\cdot n$ dependent variables at time step i+1. The ten equations needed to complete the problem are provided by boundary conditions.
The algebraic equivalents of the governing Eqs. (3)-(12) are derived using the grid transformation proposed by Eq. (17). The associated algebraic equations are given in Appendix B of the present paper. The boundary conditions which are needed to complete the final $10\cdot n$ algebraic system correspond to zero bending moments at both ends of the catenary, zero motions at the bottom fixed point and specified time depended excitations at the top in three directions. The final system is solved efficiently by the relaxation method.

5. Discussion on the contribution of the nonlinearities

The nonlinearities involved in the problem are either geometric or hydrodynamic nonlinearities. Here the current is ignored and accordingly, the hydrodynamic action is represented by the nonlinear drag forces induced due to the motions of the structure. It is noted that the presence of current could stimulate possible vortex-induced-vibration phenomena, the study of which exceeds the purposes of the present contribution. In addition the structure is slender and therefore the diffraction phenomena are negligible. This makes the drag forces the most determinative factor of hydrodynamic nature. Other hydrodynamic effects involved in the problem are the added inertia forces which are expressed through the added mass coefficients in the normal and the bi-normal directions.
Apart from the drag forces the dynamic equilibrium of the catenary involves also geometric nonlinearities. Apparently, the most important are the internal loading-curvature terms. The term "internal loading" refers to the tension and the shear forces. The question which easily arises is how nonlinear contributions influence the motions of the structure, namely the axial, the normal and the bi-normal displacements. It is evident that any excitation will induce displacements in the same direction but the question herein concerns the details of the motions which are induced in the other directions. The later remark is intimately connected with the so called "compression loading", i.e. the amplification of the bending moments at the touch down region due to the dynamic components. The importance of the subject regarding the in-plane bending moment has been extensively discussed by Passano and Larsen (2006) and Chatjigeorgiou et al. (2007). Here the discussion is extended to the out-of-plane bending moments as well.
In order to distinguish between the linear and the nonlinear effects it is indispensable to go through the equivalent linearized dynamic problem. It is assumed that the generalized loading terms and the Eulerian angles consist of a static and a dynamic component. These will be denoted in the sequel by the indexes 0 and 1 respectively. In addition small motions are considered. Thus the velocities are given by $u=\partial p/\partial t$, $v=\partial q/\partial t$ and $w=\partial r/\partial t$, where p, q

and r are the motions in the axial, normal and bi-normal directions. Thus, the vector of the unknowns of the linear problem $\vec{Y}(s;t) = [p \quad q \quad r \quad T \quad \phi \quad \theta \quad S_b \quad S_n \quad \Omega_n \quad \Omega_b]^{\mathbf{T}}$ becomes

$$\vec{Y}(s;t) = Y_0(s) + \vec{Y}_1(s;t) \tag{18}$$

where

$$Y_0(s) = [0 \quad 0 \quad 0 \quad T_0 \quad \phi_0 \quad \theta_0 \quad S_{b0} \quad S_{n0} \quad \Omega_{n0} \quad \Omega_{b0}]^{\mathbf{T}} \tag{19}$$

and

$$\vec{Y}_1(s;t) = [p \quad q \quad r \quad T_1 \quad \phi_1 \quad \theta_1 \quad S_{b1} \quad S_{n1} \quad \Omega_{n1} \quad \Omega_{b1}]^{\mathbf{T}} \tag{20}$$

The linearization procedure is outlined succinctly in the following. First, Eq. (18) is introduced into the nonlinear system of Eqs. (3)-(12). After short mathematical manipulations it can be seen that the resulting products will include the terms that define the static equilibrium problem as well as nonlinear components. Static equilibrium terms cancel each other while in the context of the linearized problem, the nonlinear terms are ignored. The compatibility relations given by Eqs. (6)-(8), are integrated with respect to time t. Finally, it is noted that the static terms Ω_{n0}, θ_0 and S_{b0} are zero. This is due to the two-dimensional static configuration of the catenary.
By employing the above procedure, the system of Eqs. (3)-(12) is reduced to the equivalent linearized system.

$$m\frac{\partial^2 p}{\partial t^2} = \frac{\partial T_1}{\partial s} - S_{n0}\Omega_{b1} - S_{n1}\Omega_{b0} - w_0 \cos\phi_0\phi_1 \tag{21}$$

$$(m + m_a)\frac{\partial^2 q}{\partial t^2} = \frac{\partial S_{n1}}{\partial s} + T_1\Omega_{b0} + \Omega_{b1}T_0 + w_0 \sin\phi_0\phi_1 - c_n\omega|q|\frac{\partial q}{\partial t} \tag{22}$$

$$(m + m_a)\frac{\partial^2 r}{\partial t^2} = \frac{\partial S_{b1}}{\partial s} - S_{n0}\Omega_{b0}\theta_1 - T_0\Omega_{n1} - w_0 \sin\phi_0\theta_1 - c_b\omega|r|\frac{\partial r}{\partial t} \tag{23}$$

$$T_1 = EA\left(\frac{\partial p}{\partial s} - \Omega_{b0}q\right) \tag{24}$$

$$\phi_1 = \frac{\partial q}{\partial s} + \Omega_{b0}p \tag{25}$$

$$\theta_1 = -\frac{\partial r}{\partial s} \tag{26}$$

$$EI\frac{\partial \Omega_{n1}}{\partial s} - EI\Omega_{b0}\theta_1 = S_{b1} \tag{27}$$

$$EI\frac{\partial \Omega_{b1}}{\partial s} = -S_{n1} \tag{28}$$

$$\frac{\partial \theta_1}{\partial s} = \Omega_{n1} \tag{29}$$

$$\frac{\partial \phi_1}{\partial s} = \Omega_{b1} \tag{30}$$

In Eqs. (22) and (23) c_n=4/(3π)$\rho C_{dn} d_o$ and c_b=4/(3π)$\rho C_{db} d_o$ denote the linearized damping coefficients which are determined through the linearization process of the nonlinear drag forces R_{dn} and R_{db}. Also, the drag force in tangential direction was considered negligible, whereas the elastic strain e was set equal to zero.

Eqs. (21)-(30) consists of two major groups, namely one set that governs the coupled axial and normal motions (Eqs. (21), (22), (24), (25), (28) and (30)) and one set that governs the bi-normal or out-of-plane motions (Eqs. (23), (26), (27) and (29)). Provided that the solution of the static equilibrium problem is known, the two systems can be treated separately, which implies that, at least in the context of the linear problem, the in-plane motions do not influence the out-of-plane motions and vise versa. Thus, the axial and normal motions induced out-of plane vibrations is only due to the nonlinear terms and especially due to the geometric nonlinearities. This can be traced back to the fact that the out-of-plane static components Ω_{n0}, S_{b0} and θ_0, were assumed equal to zero. In fact, this is the actual case when the structure is perfect with no initial deformations, even marginal, and the excitations coincide absolutely with the unit vectors $\vec{t}$ and $\vec{n}$ for the in-plane motions and $\vec{b}$ for the out of plane motions.

For the linear problem, which by default assumes that the motions are relatively small, the in-plane and out-of-plane motions and their consequences, as regards the moments, the shear forces and the tension, can be considered uncoupled without loss of accuracy. Nevertheless, this is not a valid approach for the nonlinear problem. For a perfect structure however and assuming only in-plane excitations it will be easy to confirm, through the solution of the dynamic problem, that no out-of-plane motions are induced. This is a shortcoming of the theoretical methods which is associated with the disability to represent the marginal structural imperfections of the static configuration. However it is no difficult to invent numerical tricks to override this practical problem. In the present contribution for example, the numerical results which refer to the heave excitation induced out-of-plane motions, were obtained by exciting the structure at the top with a combined motion that consists of a vertical and a bi-normal component. The later is applied for a limited amount of time, which is enough to produce non-zero out-of-plane angles, bending moments and shear forces. Thus, at the cut-off time step the structure has obtained a 3D shape that explicitly diverges from the perfect in-plane configuration and is accordingly used as the initial condition for the subsequent time steps of the numerical simulation.

6. Numerical results and discussion

The numerical results which are presented in the following refer to the SCR that was used as a model by Passano and Larsen (2006). The same model was employed also by Chatjigeorgiou (2008). The physical and geometrical properties of the structure are: outer diameter 0.429m, wall thickness 0.0022m, Young modulus of elasticity 207GPa, mass per unit unstretched length 262.9kg/m, added mass per unit unstretched length 148.16kg/m, submerged weight per unit unstretched length 915.6N/m, suspended length 2024m, elastic stiffness $0.5823 \cdot 10^{10}$N and bending stiffness $0.1209 \cdot 10^{9}$Nm^2. The drag coefficients in normal and bi-normal directions were assumed equal to unity while the tangential drag coefficient was set equal to zero. Finally, with regard to the installation characteristics, the catenary was assumed suspended in water depth 1800m by applying a pretension at the top equal to 1860kN.

This work focuses mainly on the out-of-plane dynamics of the catenary, induced due to both in-plane and out-of-plane motions. More interesting from the academic point of view is the former type of excitation as in this case the out-of-plane motions are driven by nonlinearities.

6.1 Bi-normal (sway) excitation

Normally, nonlinear phenomena are stimulated at high frequencies and large amplitudes or by combining both properties, at high excitation velocities. Therefore in order to expose and study the associated impacts, the structure should be subjected to relatively severe loading. The details of the sway excitation are examined having the structure excited with a harmonic motion at the top with amplitude y_a=1.0m and circular frequency ω=2.0rad/s.

The solution in the time domain and especially the one that accounts for the nonlinear terms calculates the time histories of all time varying components at any point along the structure, providing huge data records, which admittedly, are hard to be handled. In addition, in a nonlinear formulation the records of the output signals will contain the contribution of sub- and super-harmonics which are difficult to be identified by inspecting only the time histories. Therefore, in order to present the results in a friendly and understandable format, all records were processed using Fast Fourier Transformation (FFT) and adopted to 3D spectrums. The spectrums reveal the prevailing frequencies at any point along the catenary. For the test case mentioned before, the 3D spectrums for the dynamic tension T_1, the normal velocity v, the in-plane dynamic bending moment M_{b1}, and the out-of-plane dynamic bending moment M_{n1} are depicted respectively in Figs. 2-5. It is noted that the out-of-plane dynamic bending moment also represents the total out-of-plane bending moment as the corresponding static counterpart is zero.

Fig. 5 shows that the out-of-plane bending moment responds at the excitation frequency. This occurs for all points along the catenary. The maximum value occurs just before the top terminal point where the excitation is applied. In addition, the variation of the out-of-plane bending moment as a function of s exhibits a dentate configuration with a notable increase at the touch down area. It is also important to note that no other harmonics are stimulated and the response is restricted to the frequency of excitation only.

Figs. 2-4 demonstrate that the in-plane response due to the sway excitation is much more complicated as various harmonics are detected. The most significant contribution comes from the double of the excitation frequency (4.0rad/s) while it is visually evident that there are peaks at $1/2\omega$, $3/2\omega$, 2ω, $5/2\omega$ and so on. The non-zero values of the spectral densities for $\omega \to 0$ or $T \to \infty$, which exhibit a different pattern for the various dynamic components, imply that the sway excitation causes a quasi-static application of the corresponding component. In addition, the non-zero values for $T \to \infty$, manifest that the response is in general non periodic and it is composed by a fundamental frequency that tends to infinity and practically a boundless number of harmonics.

6.2 In-plane heave excitation induced out-of-plane response

Here a single excitation case is examined that refers to excitation amplitude in heave z_a=1.0m with circular frequency ω=1.5rad/s. Again, a relatively high excitation velocity was assumed, in order to investigate the effect of nonlinearities. In the specific static configuration the heave motion acts nearly as an axial loading which, depending on the conditions, may result in "compression loading".

The details of the in-plane and the out-of-plane response due to the applied heave excitation are examined with the aid of Figs. 6-19. Figs. 6-8 are given as a part of the discussion, started in section 5, on the dependence of the out-of-plane motions, shear forces and bending moments by the initial static configuration. Figs. 6-7 demonstrate a dependence of the concerned variables on the amplitude of the sway excitation that is applied for practical reasons and for a short time, just to provide an initial out-of-plane deformation to the structure. Apparently, the records of the response, which in the specific case correspond to the location where the maximum static bending moment M_{b0} occurs, are different for different amplitudes. Nevertheless, the output signals converge for large amplitudes. The attainment of convergence is better shown in shear force S_{b1} (Fig. 8), as in this case the associated time history contains abnormal signals which however, do not dilute periodicity. Nevertheless, it should be noted that the impotence to formulate accurately the marginal static deformations in the out-of-plane direction, which it turn leads to the necessity to apply artificially non-zero values of $M_{n0}(s)$ and $\theta_0(s)$, constitutes in this connection, a numerical uncertainty.

Next, we focus for a while in Figs. 6-8. Fig. 8 is a little bit confusing whereas a careful inspection in Fig. 7 indicates the existence of a base harmonic and an additional harmonic. The two harmonics are more evident in the time history of the out-of-plane velocity w (Fig. 6) and it can be shown that they correspond to 0.75rad/s and 2.25rad/s. In other words none of the harmonics coincides with the excitation frequency. In particular, the concerned harmonics correspond to $1/2\omega$ and $3/2\omega$ where ω is the frequency of the excitation. Apparently the occurrence of these harmonics makes the motion of the structure quite complicated. The latter remark is graphically shown in Figs. 9-11 which demonstrate the path that is followed (in particular by node no 3 in a discretization grid of 100 nodes at s=41m from touch down point) as seen from behind ($v=f(w)$), from above ($u=f(w)$) and from the side ($v=f(u)$), respectively. It is noted that in Figs. 9-11 v and u respond following the excitation frequency ω while w responds having contributions from both $1/2\omega$ and $3/2\omega$. Fig. 9 shows that the general impression that the orbit of the structure follows a reclined "eight" configuration is not absolutely true. In fact, the motion is more complicated, mainly due to the contribution of $3/2\omega$. The reclined "eight" path or using a more symbolic term the "butterfly" motion, is more appropriate to be used in order to describe the motion of the structure from above, i.e. the function $u=f(w)$. Finally, the fundamental frequency of the response for v and u which are both in-plane components is equal to the excitation frequency. This is shown with a more descriptive fashion in Fig. 11 where the function $v=f(u)$ is represented by two coinciding closed loops.

Figs. 9-11 have been plotted using the numerical predictions of two periods of the steady state response. Another way to verify that the in-plane motions conform to the frequency of excitation is to observe that the two loops of Fig. 11 practically coincide. However, this is not the case when the out-of-plane motion is considered, which it is driven by a subharmonic and a superharmonic of the excitation frequency. In this case, each of the loops in Figs. 9 and 10 (right or left) is covered during one period of the excitation. Nevertheless, the fundamental frequency for the response of w, and in general for all out-of-plane components, is the half of the excitation frequency and accordingly the steady state motion at any point along the structure is completed after two excitation periods.

The contribution of the various harmonics, which are stimulated due to the heave excitation, to both the in-plane and the out-of-plane dynamic components, is better shown in the 3D spectral densities depicted in Figs. 12-17. Figs. 12-14 show in-plane components, namely the dynamic tension T_1 (Fig. 12), the normal velocity v (Fig. 13) and the in-plane dynamic bending moment M_{b1} (Fig. 14). In the respective plots it is immediately apparent that the in-plane components are primarily governed by the excitation frequency (ω=1.5rad/s in the present case study), while it is evident that the in-plane response is affected by additional harmonics that coincide with integer multipliers of the excitation frequency ω, i.e., 2ω, 3ω etc. The 2ω superharmonic is easily detectable in all three figures, whereas 3ω is seen (admittedly with relative difficulty), only in the dynamic tension spectral density (Fig. 12). It should be stated however that it exists, together with the higher integer multipliers, in all in-plane dynamic components.

Figs. 15-17 provide the 3D spectral densities of out-of-plane dynamic components, namely the bi-normal velocity w (Fig. 15), the out-of-plane dynamic bending moment M_{n1} (Fig. 16) and the out-of-plane dynamic shear force S_{b1} (Fig. 17). For enriching the discussion that preceded with regard the dominant harmonics of the out-of-plane response due to the heave excitation, it is again underlined that the motion herein is governed by frequencies that correspond to $1/2\omega$, $3/2\omega$, $5/2\omega$ etc. The occurrence of all three of them can be detected only in Fig. 15 (again, the latter is seen with relative difficulty), while for M_{n1} and S_{b1} the response appears to be governed by $1/2\omega$. Moreover, we could positively claim that there is a slight contribution from $3/2\omega$.

The question which easily arises is what exactly these findings mean. To provide an answer we could generalize the visual observations on the 3D spectral densities of the out-of-plane components and speculate that the contributing harmonics correspond to $(n/2)\cdot\omega$ for n=1,2,…. In addition, in order to be consistent with the above discussion we could claim that the even terms of the sequence are negligible. As far as the in-plane response is concerned, the logical sequence is to assume that the constituent harmonics could be approximated by the same simple formula, but in this case, the components which could be omitted are the odd terms of the sequence.

Correlating the above findings with the Mathieu equation, should not be considered as a significant discovery as many authors did the same in the past. Nevertheless most of the works in this subject discuss vertical slender structures (risers or tethers) (Gadagi & Benaroya, 2006; Chandrasekaran et al., 2006; Kuiper et al., 2008; Park & Jung, 2002) for marine applications where the heaving motions produce buckling and the associated dynamic behaviour is directly connected to Mathieu equation. To extend the discussion in the context of catenary structures, effort has been made to associate the numerical predictions depicted graphically in 3D spectral densities to the solution(s) of Mathieu equation. The issue for which we are mainly interested is that the global response consists of harmonics $(n/2)\cdot\omega$ for n=1,2,…, or equivalently $n\cdot(2\omega)$ for n=1,2,…, provided that the excitation frequency is 2ω. The Mathieu equation which is satisfied by periodic solutions is given for reference in the following:

$$\frac{d^2y(\tau)}{d\tau^2} + (a - 2q\cos 2\tau)y(\tau) = 0 \tag{31}$$

where $\tau=\omega t$ and q is referred as the Mathieu parameter. The solutions of Mathieu Eq. (31) associated with the characteristic values a, are given by (Abramowitz & Stegun, 1970; McLachlan, 1947; Meixner & Schäfke, 1954)

$$\mathrm{ce}_{2m}(\omega t;q)=\sum_{r=0}^{\infty}A_{2r}^{2m}(q)\cos[2r\omega t] \tag{32}$$

$$\mathrm{ce}_{2m+1}(\omega t;q)=\sum_{r=0}^{\infty}A_{2r+1}^{2m+1}(q)\cos[(2r+1)\omega t] \tag{33}$$

$$\mathrm{se}_{2m+1}(\omega t;q)=\sum_{r=0}^{\infty}B_{2r+1}^{2m+1}(q)\sin[(2r+1)\omega t] \tag{34}$$

$$\mathrm{se}_{2m+2}(\omega t;q)=\sum_{r=0}^{\infty}B_{2r+2}^{2m+2}(q)\sin[(2r+2)\omega t] \tag{35}$$

where ce_m and se_m are the even and odd periodic Mathieu functions and A and B are the associated constants depending on the Mathieu parameter q. It is immediately apparent that a stable solution of Mathieu Eq. (31) will include contributions originating from an infinite number of harmonics. In any case the first harmonic will be equal to $\omega/2$ provided that the excitation frequency is ω. It is reminded that according to the numerical results that describe the in-plane and the out-of-plane dynamic behaviour of the catenary structure due to heave excitation, the response was assumed to include the same type and number of harmonics regardless whether they are significant or not. The answer to the question why the in-plane motions are governed by the harmonics ω, 2ω, 3ω,…, and the out-of-plane motions by the harmonics $\omega/2$, $3\omega/2$, $5\omega/2$,…is apparently a difficult task that requires deep and comprehensive investigation and it could be the subject for a future work.

7. Conclusion

The 3D dynamic behaviour of catenary slender structures for marine applications was considered. The investigation was based on the results obtained by solving the complete nonlinear governing system that consists of ten partial differential equations. The solution method employed was the finite differences box approximation. Particular attention was given to the out-of-plane variables which are induced due to heave excitation.

The main finding in this context was the contribution of several harmonics that influence the global response of the structure. In fact it was shown that under in-plane heave excitation at the top terminal point the in-plane variables, motions and generalized loading components, are governed by the harmonics ω, 2ω, 3ω,…, whereas the out-of-plane variables by the harmonics $\omega/2$, $3\omega/2$, $5\omega/2$,…

For the heave induced out-of-plane motions, the fundamental frequency is exactly the half of the excitation frequency. This leads to cyclic motions which are completed during a time interval that is equal to the double of the excitation period. It was shown graphically that the orbit of the structure resembles a "butterfly" configuration. This interesting behaviour was correlated to the even and odd periodic solutions of the canonical form of Mathieu equation. Finally, the contribution of the nonlinearities was studied by deriving the equivalent linearized system and it was commented that the out-of-plane motions induced due to in-plane excitation are driven by the geometric nonlinear terms.

8. References

Ablow, C.M & Schechter, S. (1983). Numerical simulation of undersea cable dynamics. *Ocean Engineering*; 10, 443-457

Abramowitz, M. & Stegun I.A. (1970). *Handbook of mathematical functions*, Dover Publications Inc, New York

Aubeny, C.P., Biscotin, G. & Zhang, J (2006). *Seafloor interaction with steel catenary risers*, Final Project Report, MMS Project No 510, Texas A&M University

Burgess, J.J. (1993). Bending stiffness in a simulation of undersea cable deployment., *International Journal of Offshore and Polar Engineering*, 3, 197-204

Chandrasekaran, S., Chandak, N.R. & Anupam, G. (2006). Stability analysis of TLP tethers, *Ocean Engineering,* 33, 471-482.

Chatjigeorgiou, I.K. & Mavrakos, S.A. (1999). Comparison of numerical methods for predicting the dynamic behavior of mooring lines. *Proceedings of the 9th International Conference on Offshore and Polar Engineering (ISOPE 1999)*, Brest, France, Vol. II, 332-339

Chatjigeorgiou, I.K. & Mavrakos, S.A. (2000). Comparative evaluation of numerical schemes for 2D mooring dynamics, *International Journal of Offshore and Polar Engineering,* 10, 301-309

Chatjigeorgiou, I.K., Passano, E. & Larsen, C.M. (2007). Extreme bending moments on long catenary risers due to heave excitation, *Proceedings of the 26th International Conference on Offshore Mechanics and Arctic Engineering (OMAE 2007)*, San Diego, California, USA, Paper No 29384.

Chatjigeorgiou, I.K. (2008). A finite differences formulation for the linear and nonlinear dynamics of 2D catenary risers, *Ocean Engineering,* 35, 616-636.

Clukey, E., Jacob, P. & Sharma, P. (2008). Investigation of riser seafloor interaction using explicit finite element methods. *Offshore Technology Conference*, Houston, Texas, OTC 19432

Gadagi, M.M. & Benaroya, H. (2006). Dynamic response of an axially loaded tendon of a tension leg platform, *Journal of Sound and Vibration,* 293, 38-58.

Gobat, J.I. & Grosenbaugh, M.A. (2001). Application of the generalized-*a* method to the time integration of the cable dynamics equations, *Computer Methods in Applied Mechanics and Engineering,* 190, 4817-4829.

Gobat, J.I., Grosenbaugh, M.A. & Triantafyllou, M.S. (2002). Generalized-*a* time integration solutions for hanging chain dynamics. *Journal of Engineering Mechanics – ASCE,* 128, 677-687

Gobat, J.I. & Grosenbaugh, M.A. (2006). Time-domain numerical simulation of ocean cable structures, *Ocean Engineering,* 33, 1373-1400.

Hoffman, J.D. (1993). *Numerical methods for engineers and scientists,* McGraw-Hill, New York

Howell, C.T. (1991). Numerical analysis of 2-D nonlinear cable equations with applications to low tension problems, *Proceedings of the 1st International Offshore and Polar Engineering Conference (ISOPE 1991)*, Edinburgh, United Kingdom, Vol. II, 203-209.

Howell, C.T. *Investigation of the dynamics of low tension cables*, PhD Thesis, Massachusetts Institute of Technology, Cambridge, Massachusetts

ISSC (2003). *Report of the committee V.5: Floating Production Systems*. Elsevier Science, Oxford, Eds A.E. Mansour, R.C. Ertekin.

Jain, A.K. Review of flexible risers and articulated storage systems, *Ocean Engineering,* 21, 733-750.

Kuiper, G.L. & Metrikine, AV. (2005). Dynamic stability of a submerged, free-hanging riser conveying fluid, *Journal of Sound and Vibration,* 280, 1051–1065.

Kuiper, G.L., Brugmans, J. & Metrikine, AV. (2008). Destabilization of deep-water risers by a heaving platform, *Journal of Sound and Vibration,* 310, 541-557.

LeCunff, C., Biolley, F. & Damy, G. (2005). Experimental and numerical study of heave induced lateral motion (HILM), *Proceedings of the 24th International Conference on Offshore Mechanics and Arctic Engineering (OMAE 2005)*, Halkidiki, Greece, Paper No 67019

Leira, B.J., Karunakaran, D., Giertsen, E., Passano, E. & Farnes, K-A. Analysis guidelines and application of a riser-soil interaction model including trench effects, *Proceedings of the 23rd International Conference on Offshore Mechanics and Arctic Engineering (OMAE 2004)*, Vancouver, Canada, Paper No 51527

McLachlan N.W. (1947). *Theory and applications of Mathieu functions*, Dover Publications, New York.

Meixner J. & Schäfke F.W. (1954). *Mathieusche funktionen und sphäroidfunktionen,* Springer, Berlin

Milinazzo, F., Wilkie, M. & Latchman, S.A. (1987). An efficient algorithm for simulating the dynamics of towed cable systems, *Ocean Engineering,* 14, 513-526.

Park, H-I., & Jung, D-H. (2002). A finite element method for dynamic analysis of long slender marine structures under combined parametric and forcing excitations, *Ocean Engineering,* 29, 1313-1325.

Passano, E. & Larsen, C.M. (2006). Efficient analysis of a catenary riser, *Proceedings of the 25th International Conference on Offshore Mechanics and Arctic Engineering (OMAE 2006)*, Hamburg, Germany, Paper No 92308

Passano, E. & Larsen, C.M. (2007). Estimating distributions for extreme response of a catenary riser. *Proceedings of the 26th International Conference on Offshore Mechanics and Arctic Engineering (OMAE 2007)*, San Diego, California, USA, Paper No 29547.

Patel, H.M. & Seyed, F.B. (1995). Review of flexible risers modelling and analysis techniques, *Engineering Structures,* 17, 293-304.

Pesce, C.P., Martins, C.A. & Silveira, L.M.Y. (2006). Riser-soil interaction: Local dynamics at TDP and a discussion on the eigenvalue and the VIV problems, *Journal of Offshore Mechanics and Arctic Engineering,* 128, 39-55.

Tjavaras, A.A., Zhu, Q., Liu, Y., Triantafyllou, M.S. & Yue, D.K.P. (1998). The mechanics of highly extensible cables, *Journal of Sound and Vibration,* 213, 709-737

Triantafyllou, M.S. (1994). Cable mechanics for moored floating structures. *Proceedings of the 7th International Conference on the Behaviour of Offshore Structures (BOSS 1994)*, Boston, Massachusetts, Vol. 2, 57-77.

Zare, K. & Datta, T.K. (1988). Vibration of Lazy-"S" risers due to vortex shedding under lock-in, *Proceedings of the 20th Offshore Technology Conference*, OTC 5795.

Appendix A. Mass matrix M, stiffness matrix K and forcing vector F of Eq. (16)

$$\mathrm{M}=\begin{bmatrix} -m & 0 & 0 & 0 & mv\cos\theta & -mw & 0 & 0 & 0 & 0 \\ 0 & -m-m_a & 0 & 0 & -m(u\cos\theta+w\sin\theta) & 0 & 0 & 0 & 0 & 0 \\ 0 & 0 & -m-m_a & 0 & mv\sin\theta & mu & 0 & 0 & 0 & 0 \\ 0 & 0 & 0 & -\dfrac{1}{EA} & 0 & 0 & 0 & 0 & 0 & 0 \\ 0 & 0 & 0 & 0 & -\left(1+\dfrac{T}{EA}\right)\cos\theta & 0 & 0 & 0 & 0 & 0 \\ 0 & 0 & 0 & 0 & 0 & \left(1+\dfrac{T}{EA}\right) & 0 & 0 & 0 & 0 \\ 0 & 0 & 0 & 0 & 0 & 0 & 0 & 0 & 0 & 0 \\ 0 & 0 & 0 & 0 & 0 & 0 & 0 & 0 & 0 & 0 \\ 0 & 0 & 0 & 0 & 0 & 0 & 0 & 0 & 0 & 0 \\ 0 & 0 & 0 & 0 & 0 & 0 & 0 & 0 & 0 & 0 \end{bmatrix} \tag{A.1}$$

$$\mathrm{K}=\begin{bmatrix} 0 & 0 & 0 & 1 & 0 & 0 & 0 & 0 & 0 & 0 \\ 0 & 0 & 0 & 0 & 0 & 0 & 0 & 1 & 0 & 0 \\ 0 & 0 & 0 & 0 & 0 & 0 & 1 & 0 & 0 & 0 \\ 1 & 0 & 0 & 0 & 0 & 0 & 0 & 0 & 0 & 0 \\ 0 & 1 & 0 & 0 & 0 & 0 & 0 & 0 & 0 & 0 \\ 0 & 0 & 1 & 0 & 0 & 0 & 0 & 0 & 0 & 0 \\ 0 & 0 & 0 & 0 & 0 & 0 & 0 & 0 & EI & 0 \\ 0 & 0 & 0 & 0 & 0 & 0 & 0 & 0 & 0 & EI \\ 0 & 0 & 0 & 0 & 0 & 1 & 0 & 0 & 0 & 0 \\ 0 & 0 & 0 & 0 & \cos\theta & 0 & 0 & 0 & 0 & 0 \end{bmatrix} \tag{A.2}$$

$$\mathrm{F}=\begin{bmatrix} S_b\Omega_n - S_n\Omega_b - w_0\sin\phi\cos\theta + R_{dt} \\ \Omega_b\left(T+S_b\tan\theta\right) - w_0\cos\phi + R_{dn} + m_a\dfrac{\partial U_n}{\partial t} \\ -S_n\Omega_b\tan\theta - T\Omega_n - w_0\sin\phi\sin\theta + R_{db} + m_a\dfrac{\partial U_b}{\partial t} \\ \Omega_n w - \Omega_b v \\ \Omega_b\left(u + w\tan\theta\right) \\ -\Omega_b v\tan\theta - \Omega_n u \\ EI\Omega_b^2\tan\theta + S_b\left(1+\dfrac{T}{EA}\right)^3 \\ EI\Omega_n\Omega_b\tan\theta - S_b\left(1+\dfrac{T}{EA}\right)^3 \\ -\Omega_n \\ -\Omega_b \end{bmatrix} \tag{A.3}$$

Appendix B. Algebraic expansions of the nonlinear system of dynamic equilibrium Eqs. (3)-(12) using the finite differences box scheme

$$
\begin{aligned}
E_1 &= \frac{T_k^{i+1} + T_k^i - T_{k-1}^{i+1} - T_{k-1}^i}{2\Delta s} + \frac{1}{4}\left(S_{bk}^{\ i+1}\Omega_{nk}^{\ i+1} + S_{bk}^{\ i}\Omega_{nk}^{\ i} + S_{bk-1}^{\ i+1}\Omega_{nk-1}^{\ i+1} + S_{bk-1}^{\ i}\Omega_{nk-1}^{\ i}\right) \\
&- \frac{1}{4}\left(S_{nk}^{\ i+1}\Omega_{bk}^{\ i+1} + S_{nk}^{\ i}\Omega_{bk}^{\ i} + S_{nk-1}^{\ i+1}\Omega_{bk-1}^{\ i+1} + S_{nk-1}^{\ i}\Omega_{bk-1}^{\ i}\right) \\
&- \frac{w_0}{4}\left(\sin\phi_k^{i+1}\cos\theta_k^{i+1} + \sin\phi_k^i\cos\theta_k^i + \sin\phi_{k-1}^{i+1}\cos\theta_{k-1}^{i+1} + \sin\phi_{k-1}^i\cos\theta_{k-1}^i\right) \\
&- \frac{1}{2}\pi\rho d_o C_{dt}\frac{1}{4}\Bigg[v_{trk}^{\ i+1}\left|v_{trk}^{\ i+1}\right|\left(1+e_k^{i+1}\right)^{1/2} + v_{trk}^{\ i}\left|v_{trk}^{\ i}\right|\left(1+e_k^i\right)^{1/2} \\
&v_{trk-1}^{\ i+1}\left|v_{trk-1}^{\ i+1}\right|\left(1+e_{k-1}^{i+1}\right)^{1/2} + v_{trk-1}^{\ i}\left|v_{trk-1}^{\ i}\right|\left(1+e_{k-1}^i\right)^{1/2}\Bigg] \\
&- m\Bigg[\frac{u_k^{i+1} + u_{k-1}^{i+1} - u_k^i - u_{k-1}^i}{2\Delta t} + \frac{1}{4}\left(w_k^{i+1} + w_{k-1}^{i+1} + w_k^i + w_{k-1}^i\right)\frac{\theta_k^{i+1} + \theta_{k-1}^{i+1} - \theta_k^i - \theta_{k-1}^i}{2\Delta t} \\
&- \frac{1}{4}\left(v_k^{i+1}\cos\theta_k^{i+1} + v_k^i\cos\theta_k^i + v_{k-1}^{i+1}\cos\theta_{k-1}^{i+1} + v_{k-1}^i\cos\theta_{k-1}^i\right)\frac{\phi_k^{i+1} + \phi_{k-1}^{i+1} - \phi_k^i - \phi_{k-1}^i}{2\Delta t}\Bigg] = 0
\end{aligned}
\tag{B.1}
$$

$$
\begin{aligned}
E_2 &= \frac{S_{nk}^{\ i+1} + S_{nk}^{\ i} - S_{nk-1}^{\ i+1} - S_{nk-1}^{\ i}}{2\Delta s} + \frac{1}{4}\left(T_k^{i+1}\Omega_{bk}^{\ i+1} + T_k^i\Omega_{bk}^{\ i} + T_{k-1}^{i+1}\Omega_{bk-1}^{\ i+1} + T_{k-1}^i\Omega_{bk-1}^{\ i}\right) \\
&+ \frac{1}{4}\left(\Omega_{bk}^{\ i+1}S_{bk}^{\ i+1}\tan\theta_k^{i+1} + \Omega_{bk}^{\ i}S_{bk}^{\ i}\tan\theta_k^i + \Omega_{bk-1}^{\ i+1}S_{bk-1}^{\ i+1}\tan\theta_{k-1}^{i+1} + \Omega_{bk-1}^{\ i}S_{bk-1}^{\ i}\tan\theta_{k-1}^i\right) \\
&- \frac{w_0}{4}\left(\cos\phi_k^{i+1} + \cos\phi_k^i + \cos\phi_{k-1}^{i+1} + \cos\phi_{k-1}^i\right) \\
&- \frac{1}{2}\rho d_o C_{dn}\frac{1}{4}\Bigg[v_{nrk}^{\ i+1}\left|\left(v_{nrk}^{\ i+1}\right)^2 + \left(v_{brk}^{\ i+1}\right)^2\right|^{1/2}\left(1+e_k^{i+1}\right)^{1/2} + v_{nrk}^{\ i}\left|\left(v_{nrk}^{\ i}\right)^2 + \left(v_{brk}^{\ i}\right)^2\right|^{1/2}\left(1+e_k^i\right)^{1/2} \\
&v_{nrk-1}^{\ i+1}\left|\left(v_{nrk-1}^{\ i+1}\right)^2 + \left(v_{brk-1}^{\ i+1}\right)^2\right|^{1/2}\left(1+e_{k-1}^{i+1}\right)^{1/2} + v_{nrk-1}^{\ i}\left|\left(v_{nrk-1}^{\ i}\right)^2 + \left(v_{brk-1}^{\ i}\right)^2\right|^{1/2}\left(1+e_{k-1}^i\right)^{1/2}\Bigg] \\
&- m\frac{v_k^{i+1} + v_{k-1}^{i+1} - v_k^i - v_{k-1}^i}{2\Delta t} - m_a\frac{v_{nrk}^{\ i+1} + v_{nrk-1}^{\ i+1} - v_{nrk}^{\ i} - v_{nrk-1}^{\ i}}{2\Delta t} \\
&- \frac{m}{4}\left(u_k^{i+1}\cos\theta_k^{i+1} + u_k^i\cos\theta_k^i + u_{k-1}^{i+1}\cos\theta_{k-1}^{i+1} + u_{k-1}^i\cos\theta_{k-1}^i\right)\frac{\phi_k^{i+1} + \phi_{k-1}^{i+1} - \phi_k^i - \phi_{k-1}^i}{2\Delta t} \\
&- \frac{m}{4}\left(w_k^{i+1}\sin\theta_k^{i+1} + w_k^i\sin\theta_k^i + w_{k-1}^{i+1}\sin\theta_{k-1}^{i+1} + w_{k-1}^i\sin\theta_{k-1}^i\right)\frac{\phi_k^{i+1} + \phi_{k-1}^{i+1} - \phi_k^i - \phi_{k-1}^i}{2\Delta t} = 0
\end{aligned}
\tag{B.2}
$$

$$
\begin{aligned}
E_3 &= \frac{S_{bk}^{i+1} + S_{bk}^{i} - S_{bk-1}^{i+1} - S_{bk-1}^{i}}{2\Delta s} - \frac{1}{4}\left(T_k^{i+1}\Omega_{nk}^{i+1} + T_k^{i}\Omega_{nk}^{i} + T_{k-1}^{i+1}\Omega_{nk-1}^{i+1} + T_{k-1}^{i}\Omega_{nk-1}^{i}\right) \\
&- \frac{1}{4}\left(\Omega_{bk}^{i+1}S_{nk}^{i+1}\tan\theta_k^{i+1} + \Omega_{bk}^{i}S_{nk}^{i}\tan\theta_k^{i} + \Omega_{bk-1}^{i+1}S_{nk-1}^{i+1}\tan\theta_{k-1}^{i+1} + \Omega_{bk-1}^{i}S_{nk-1}^{i}\tan\theta_{k-1}^{i}\right) \\
&- \frac{w_0}{4}\left(\sin\phi_k^{i+1}\sin\theta_k^{i+1} + \sin\phi_k^{i}\sin\theta_k^{i} + \sin\phi_{k-1}^{i+1}\sin\theta_{k-1}^{i+1} + \sin\phi_{k-1}^{i}\sin\theta_{k-1}^{i}\right) \\
&- \frac{1}{2}\rho d_o C_{db}\frac{1}{4}\Bigg[v_{brk}^{i+1}\left|\left(v_{nrk}^{i+1}\right)^2 + \left(v_{brk}^{i+1}\right)^2\right|^{1/2}\left(1+e_k^{i+1}\right)^{1/2} + v_{brk}^{i}\left|\left(v_{nrk}^{i}\right)^2 + \left(v_{brk}^{i}\right)^2\right|^{1/2}\left(1+e_k^{i}\right)^{1/2} \\
&\quad v_{brk-1}^{i+1}\left|\left(v_{nrk-1}^{i+1}\right)^2 + \left(v_{brk-1}^{i+1}\right)^2\right|^{1/2}\left(1+e_{k-1}^{i+1}\right)^{1/2} + v_{brk-1}^{i}\left|\left(v_{nrk-1}^{i}\right)^2 + \left(v_{brk-1}^{i}\right)^2\right|^{1/2}\left(1+e_{k-1}^{i}\right)^{1/2}\Bigg] \\
&- m\frac{w_k^{i+1} + w_{k-1}^{i+1} - w_k^{i} - w_{k-1}^{i}}{2\Delta t} - m_a\frac{v_{brk}^{i+1} + v_{brk-1}^{i+1} - v_{brk}^{i} - v_{brk-1}^{i}}{2\Delta t} \\
&+ \frac{m}{4}\left(v_k^{i+1}\sin\theta_k^{i+1} + v_k^{i}\sin\theta_k^{i} + v_{k-1}^{i+1}\sin\theta_{k-1}^{i+1} + v_{k-1}^{i}\sin\theta_{k-1}^{i}\right)\frac{\phi_k^{i+1} + \phi_{k-1}^{i+1} - \phi_k^{i} - \phi_{k-1}^{i}}{2\Delta t} \\
&+ \frac{m}{4}\left(u_k^{i+1} + u_{k-1}^{i+1} + u_k^{i} + u_{k-1}^{i}\right)\frac{\theta_k^{i+1} + \theta_{k-1}^{i+1} - \theta_k^{i} - \theta_{k-1}^{i}}{2\Delta t} = 0
\end{aligned}
\tag{B.3}
$$

$$
\begin{aligned}
E_4 &= \frac{u_k^{i+1} + u_k^{i} - u_{k-1}^{i+1} - u_{k-1}^{i}}{2\Delta s} + \frac{1}{4}\left(w_k^{i+1}\Omega_{nk}^{i+1} + w_k^{i}\Omega_{nk}^{i} + w_{k-1}^{i+1}\Omega_{nk-1}^{i+1} + w_{k-1}^{i}\Omega_{nk-1}^{i}\right) \\
&- \frac{1}{4}\left(v_k^{i+1}\Omega_{bk}^{i+1} + v_k^{i}\Omega_{bk}^{i} + v_{k-1}^{i+1}\Omega_{bk-1}^{i+1} + v_{k-1}^{i}\Omega_{bk-1}^{i}\right) - \frac{1}{EA}\frac{T_k^{i+1} + T_{k-1}^{i+1} - T_k^{i} - T_{k-1}^{i}}{2\Delta t} = 0
\end{aligned}
\tag{B.4}
$$

$$
\begin{aligned}
E_5 &= \frac{v_k^{i+1} + v_k^{i} - v_{k-1}^{i+1} - v_{k-1}^{i}}{2\Delta s} + \frac{1}{4}\left(u_k^{i+1}\Omega_{bk}^{i+1} + u_k^{i}\Omega_{bk}^{i} + u_{k-1}^{i+1}\Omega_{bk-1}^{i+1} + u_{k-1}^{i}\Omega_{bk-1}^{i}\right) \\
&+ \frac{1}{4}\left(w_k^{i+1}\Omega_{bk}^{i+1}\tan\theta_k^{i+1} + w_k^{i}\Omega_{bk}^{i}\tan\theta_k^{i} + w_{k-1}^{i+1}\Omega_{bk-1}^{i+1}\tan\theta_{k-1}^{i+1} + w_{k-1}^{i}\Omega_{bk-1}^{i}\tan\theta_{k-1}^{i}\right) \\
&- \frac{1}{4}\Big[\left(1+e_k^{i+1}\right)\cos\theta_k^{i+1} + \left(1+e_k^{i}\right)\cos\theta_k^{i} + \left(1+e_{k-1}^{i+1}\right)\cos\theta_{k-1}^{i+1} \\
&+ \left(1+e_{k-1}^{i}\right)\cos\theta_{k-1}^{i}\Big]\frac{\phi_k^{i+1} + \phi_{k-1}^{i+1} - \phi_k^{i} - \phi_{k-1}^{i}}{2\Delta t} = 0
\end{aligned}
\tag{B.5}
$$

$$
\begin{aligned}
E_6 &= \frac{w_k^{i+1} + w_k^{i} - w_{k-1}^{i+1} - w_{k-1}^{i}}{2\Delta s} - \frac{1}{4}\left(u_k^{i+1}\Omega_{nk}^{i+1} + u_k^{i}\Omega_{nk}^{i} + u_{k-1}^{i+1}\Omega_{nk-1}^{i+1} + u_{k-1}^{i}\Omega_{nk-1}^{i}\right) \\
&- \frac{1}{4}\left(v_k^{i+1}\Omega_{bk}^{i+1}\tan\theta_k^{i+1} + v_k^{i}\Omega_{bk}^{i}\tan\theta_k^{i} + v_{k-1}^{i+1}\Omega_{bk-1}^{i+1}\tan\theta_{k-1}^{i+1} + v_{k-1}^{i}\Omega_{bk-1}^{i}\tan\theta_{k-1}^{i}\right) \\
&+ \frac{1}{4}\Big[\left(1+e_k^{i+1}\right) + \left(1+e_k^{i}\right) + \left(1+e_{k-1}^{i+1}\right) + \left(1+e_{k-1}^{i}\right)\Big]\frac{\theta_k^{i+1} + \theta_{k-1}^{i+1} - \theta_k^{i} - \theta_{k-1}^{i}}{2\Delta t} = 0
\end{aligned}
\tag{B.6}
$$

$$E_7 = EI\frac{\Omega_{nk}^{i+1} + \Omega_{nk}^{i} - \Omega_{nk-1}^{i+1} - \Omega_{nk-1}^{i}}{2\Delta s} - \frac{EI}{4}\Big(\Omega_{bk}^{i+1}\Omega_{bk}^{i+1}\tan\theta_k^{i+1} + \Omega_{bk}^{i}\Omega_{bk}^{i}\tan\theta_k^{i}$$
$$+ \Omega_{bk-1}^{i+1}\Omega_{bk-1}^{i+1}\tan\theta_{k-1}^{i+1} + \Omega_{bk-1}^{i}\Omega_{bk-1}^{i}\tan\theta_{k-1}^{i}\Big) \tag{B.7}$$
$$-\frac{1}{4}\left[S_{bk}^{i+1}\left(1+e_k^{i+1}\right)^3 + S_{bk}^{i}\left(1+e_k^{i}\right)^3 + S_{bk-1}^{i+1}\left(1+e_{k-1}^{i+1}\right)^3 + S_{bk-1}^{i}\left(1+e_{k-1}^{i}\right)^3\right] = 0$$

$$E_8 = EI\frac{\Omega_{bk}^{i+1} + \Omega_{bk}^{i} - \Omega_{bk-1}^{i+1} - \Omega_{bk-1}^{i}}{2\Delta s} - \frac{EI}{4}\Big(\Omega_{nk}^{i+1}\Omega_{bk}^{i+1}\tan\theta_k^{i+1} + \Omega_{nk}^{i}\Omega_{bk}^{i}\tan\theta_k^{i}$$
$$+ \Omega_{nk-1}^{i+1}\Omega_{bk-1}^{i+1}\tan\theta_{k-1}^{i+1} + \Omega_{nk-1}^{i}\Omega_{bk-1}^{i}\tan\theta_{k-1}^{i}\Big) \tag{B.8}$$
$$+\frac{1}{4}\left[S_{nk}^{i+1}\left(1+e_k^{i+1}\right)^3 + S_{nk}^{i}\left(1+e_k^{i}\right)^3 + S_{nk-1}^{i+1}\left(1+e_{k-1}^{i+1}\right)^3 + S_{nk-1}^{i}\left(1+e_{k-1}^{i}\right)^3\right] = 0$$

$$E_9 = \frac{\theta_k^{i+1} + \theta_k^{i} - \theta_{k-1}^{i+1} - \theta_{k-1}^{i}}{2\Delta s} - \frac{1}{4}\left(\Omega_{nk}^{i+1} + \Omega_{nk}^{i} + \Omega_{nk-1}^{i+1} + \Omega_{nk-1}^{i}\right) = 0 \tag{B.9}$$

$$E_{10} = \frac{1}{4}\left(\cos\theta_k^{i+1} + \cos\theta_k^{i} + \cos\theta_{k-1}^{i+1} + \cos\theta_{k-1}^{i}\right)\frac{\phi_k^{i+1} + \phi_k^{i} - \phi_{k-1}^{i+1} - \phi_{k-1}^{i}}{2\Delta s}$$
$$-\frac{1}{4}\left(\Omega_{bk}^{i+1} + \Omega_{bk}^{i} + \Omega_{bk-1}^{i+1} + \Omega_{bk-1}^{i}\right) = 0 \tag{B.10}$$

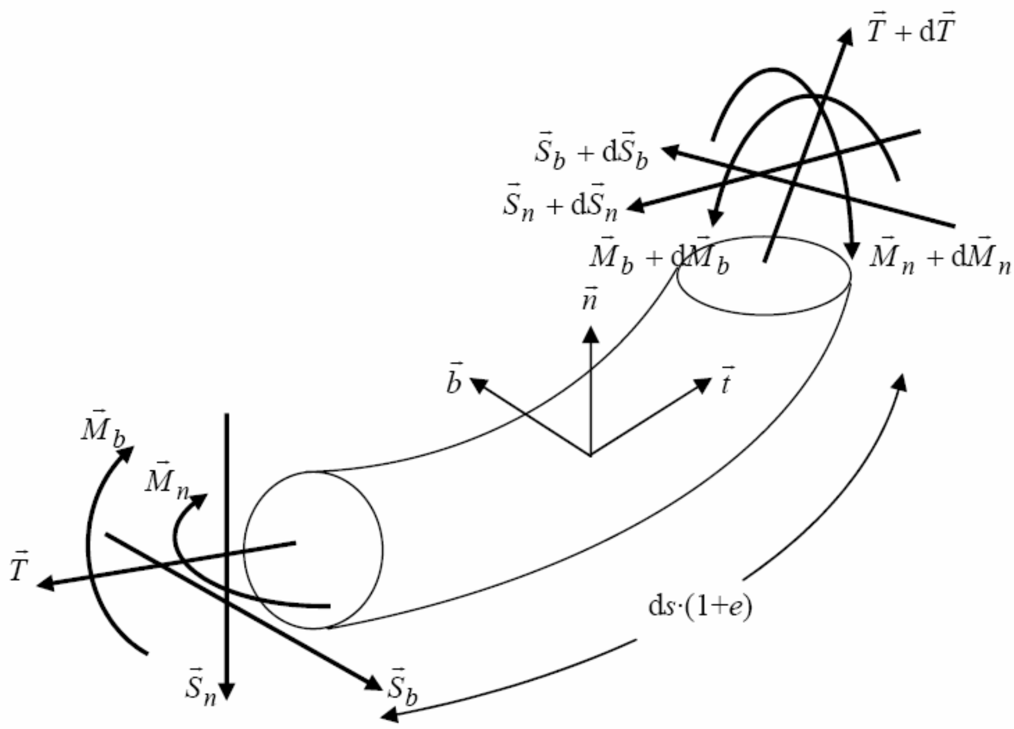

Fig. 1. Stretched catenary segment and balance of internal loading.

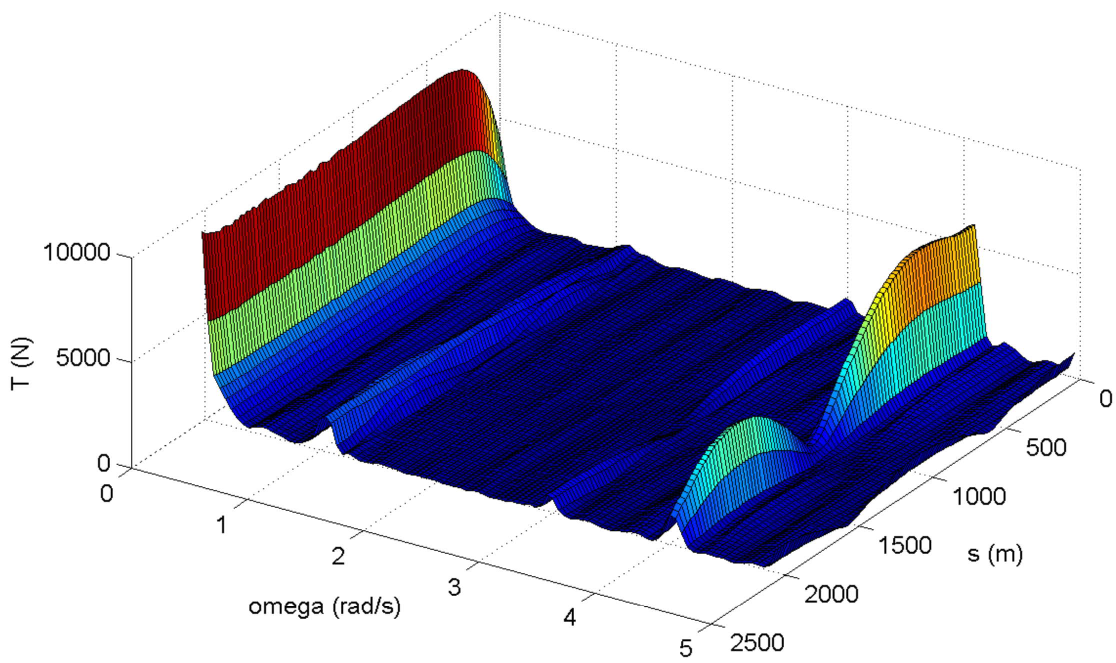

Fig. 2. Spectral densities of the dynamic tension T_1 along the catenary under sway excitation at the top, with amplitude y_a=1.0m and circular frequency ω=2.0rad/s.

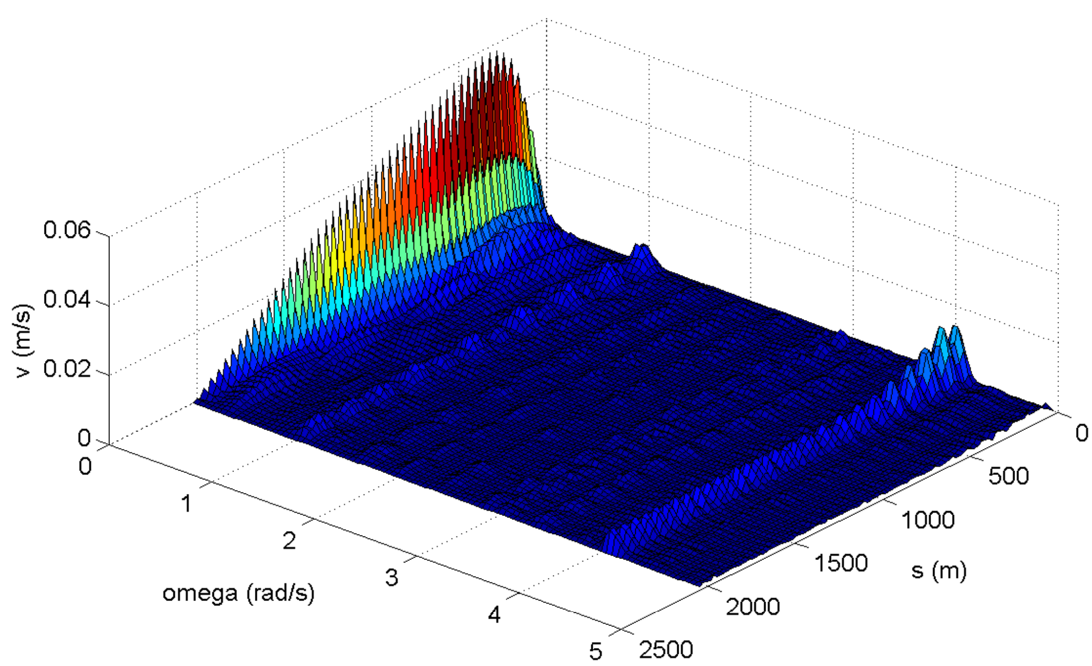

Fig. 3. Spectral densities of the normal velocity v along the catenary under sway excitation at the top, with amplitude y_a=1.0m and circular frequency ω=2.0rad/s.

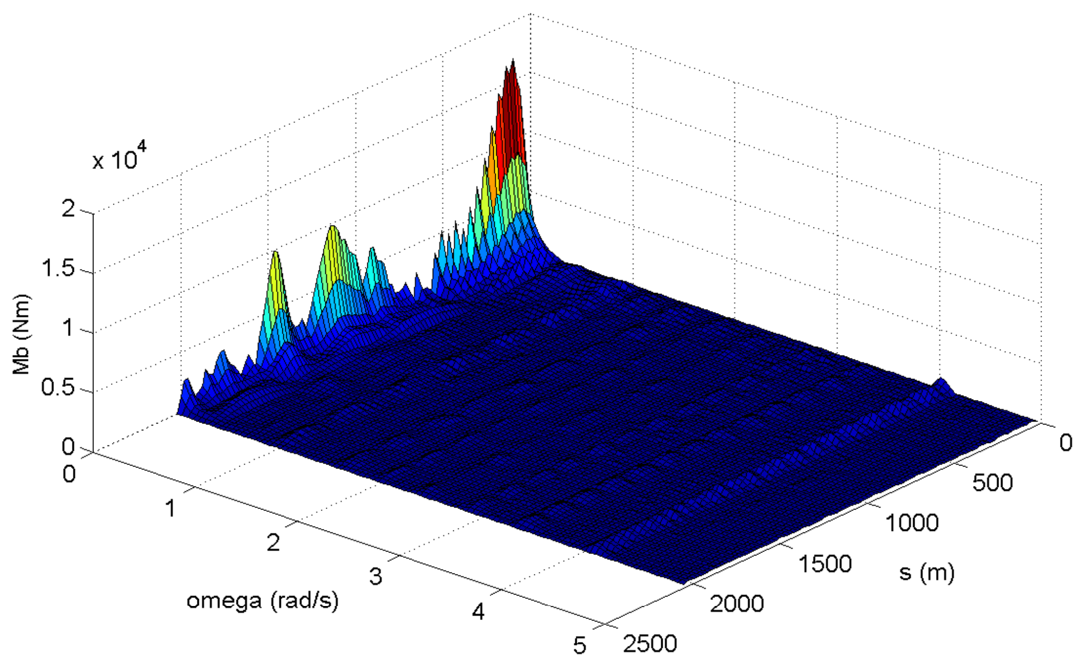

Fig. 4. Spectral densities of the in-plane dynamic bending moment M_{b1} along the catenary under sway excitation at the top, with amplitude y_a=1.0m and circular frequency ω=2.0rad/s.

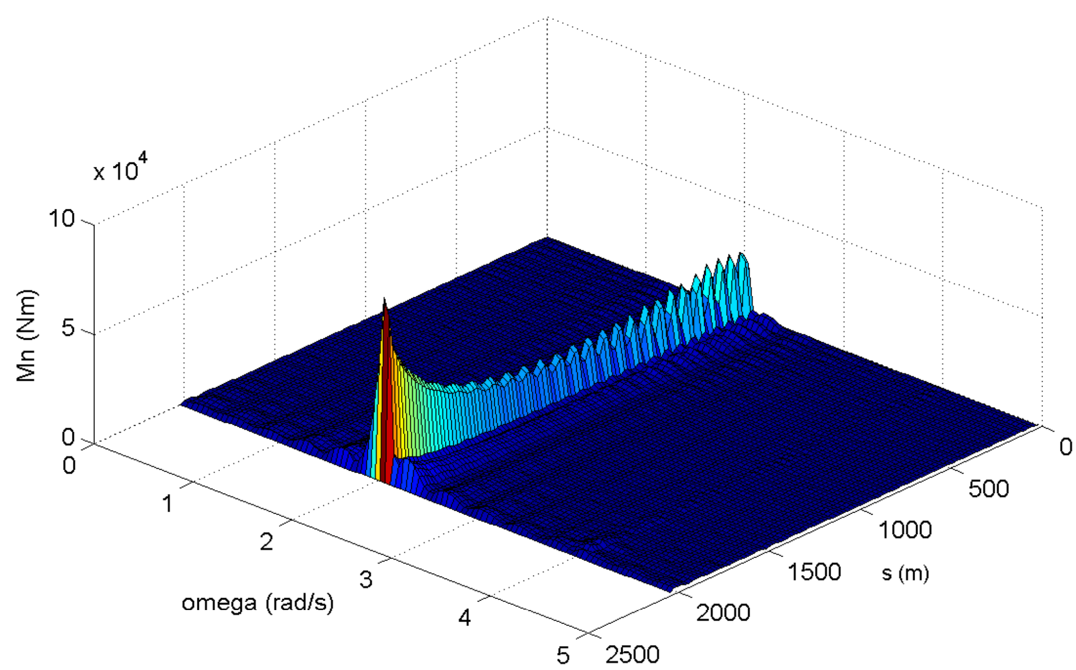

Fig. 5. Spectral densities of the out-of-plane dynamic bending moment M_{n1} along the catenary under sway excitation at the top, with amplitude y_a=1.0m and circular frequency ω=2.0rad/s.

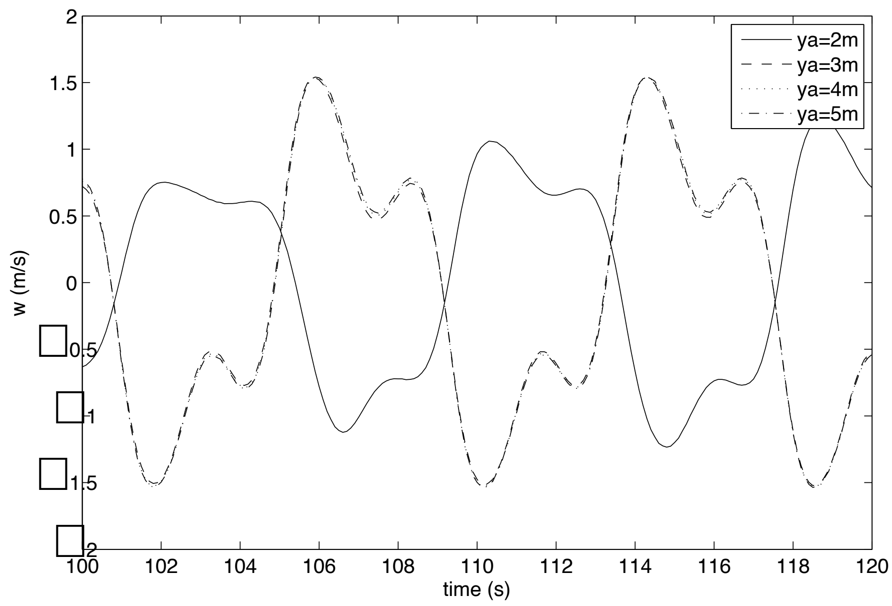

Fig. 6. Effect of the initial, short-time, sway displacement on the out-of-plane velocity w due to heave excitation with amplitude z_a=1.0m and circular frequency ω=1.5rad/s. The time history depicts the variation of w at the location of the max static in-plane bending moment M_{b0}, namely at s≈41m from touch down (at node k=3 in a discretization grid of 100 nodes)

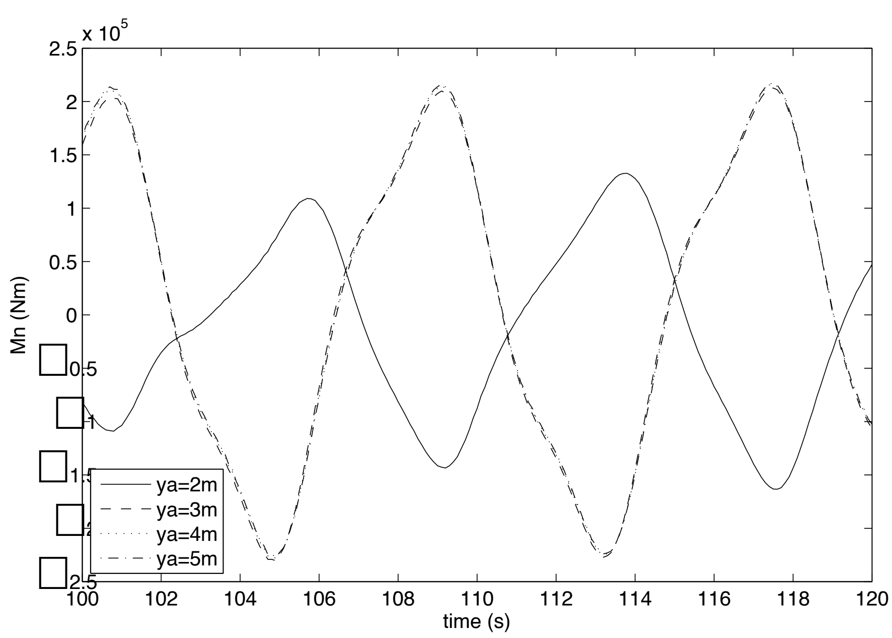

Fig. 7. Effect of the initial, short-time, sway displacement on the out-of-plane dynamic bending moment M_{n1} due to heave excitation with amplitude z_a=1.0m and circular frequency ω=1.5rad/s. The time history depicts the variation of M_{n1} at the location of the max static in-plane bending moment M_{b0}, namely at s≈41m from touch down (at node k=3 in a discretization grid of 100 nodes)

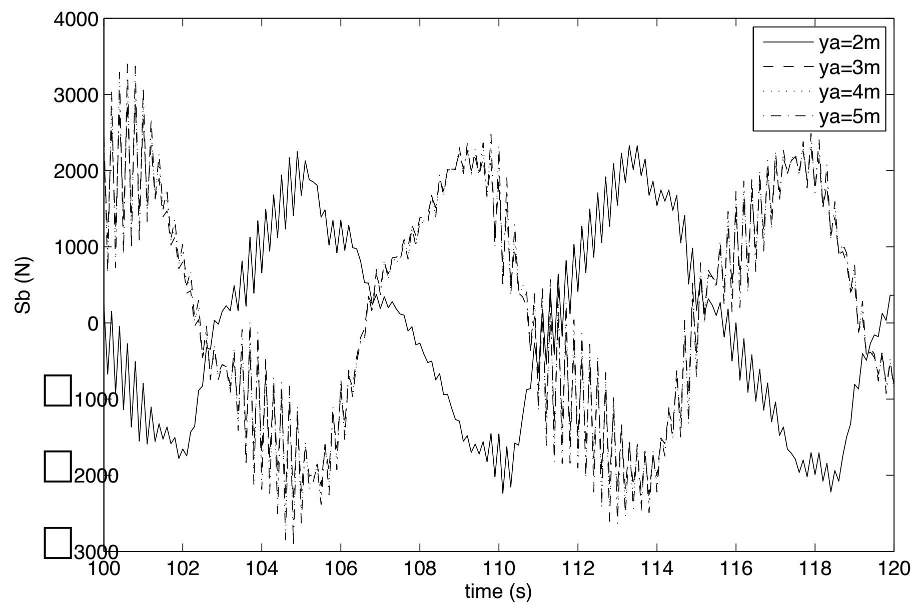

Fig. 8. Effect of the initial, short-time, sway displacement on the out-of-plane dynamic shear force S_{b1} due to heave excitation with amplitude z_a=1.0m and circular frequency ω=1.5rad/s. The time history depicts the variation of S_{b1} at the location of the max static in-plane bending moment M_{b0}, namely at $s\approx$41m from touch down (at node k=3 in a discretization grid of 100 nodes)

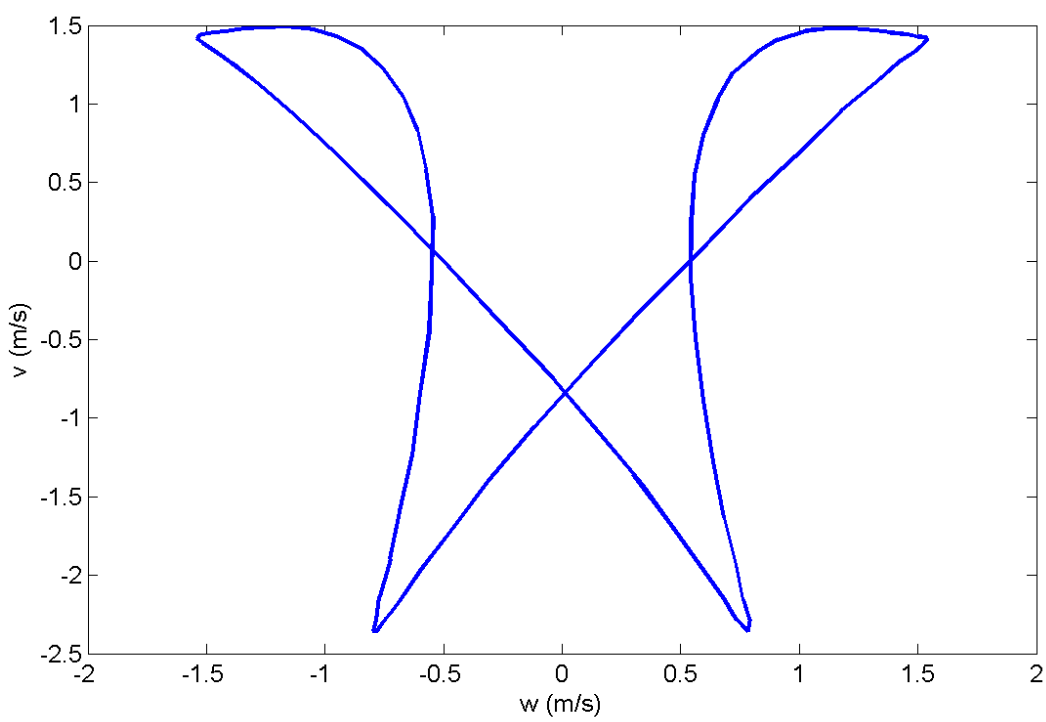

Fig. 9. Orbit of node no 3 (in a discretization grid of 100 nodes at s=41m from touch down) as seen from behind (v=$f(w)$), under heave excitation at the top with amplitude z_a=1.0m and circular frequency ω=1.5rad/s.

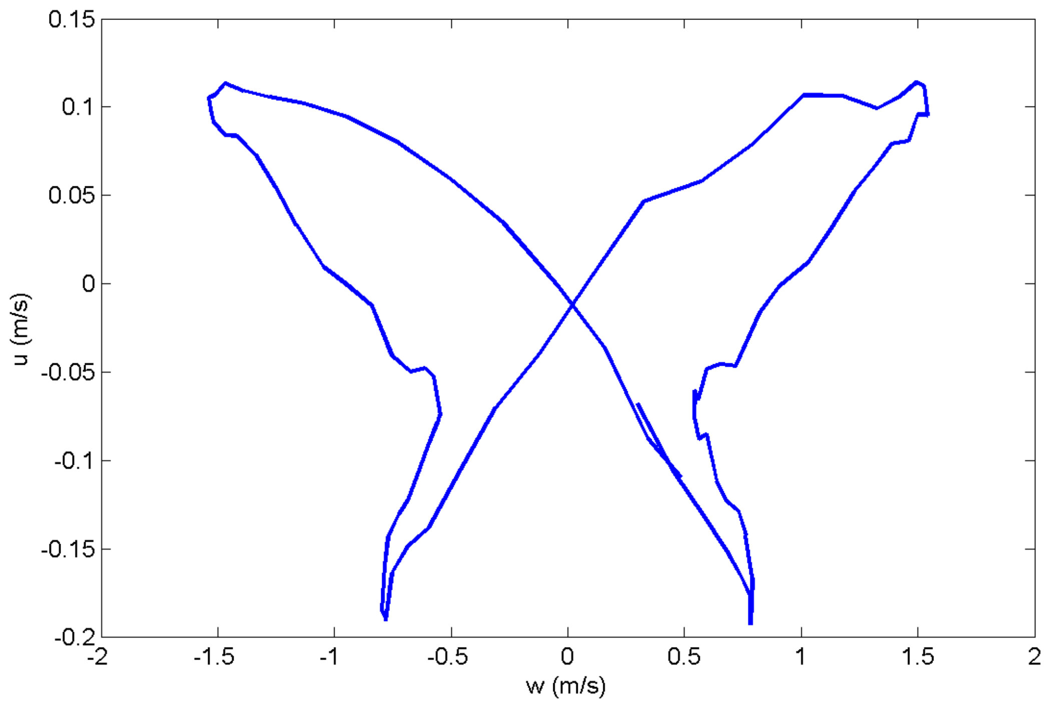

Fig. 10. Orbit of node no 3 (in a discretization grid of 100 nodes at *s*=41m from touch down) as seen from above ($u=f(w)$), under heave excitation at the top with amplitude z_a=1.0m and circular frequency ω=1.5rad/s.

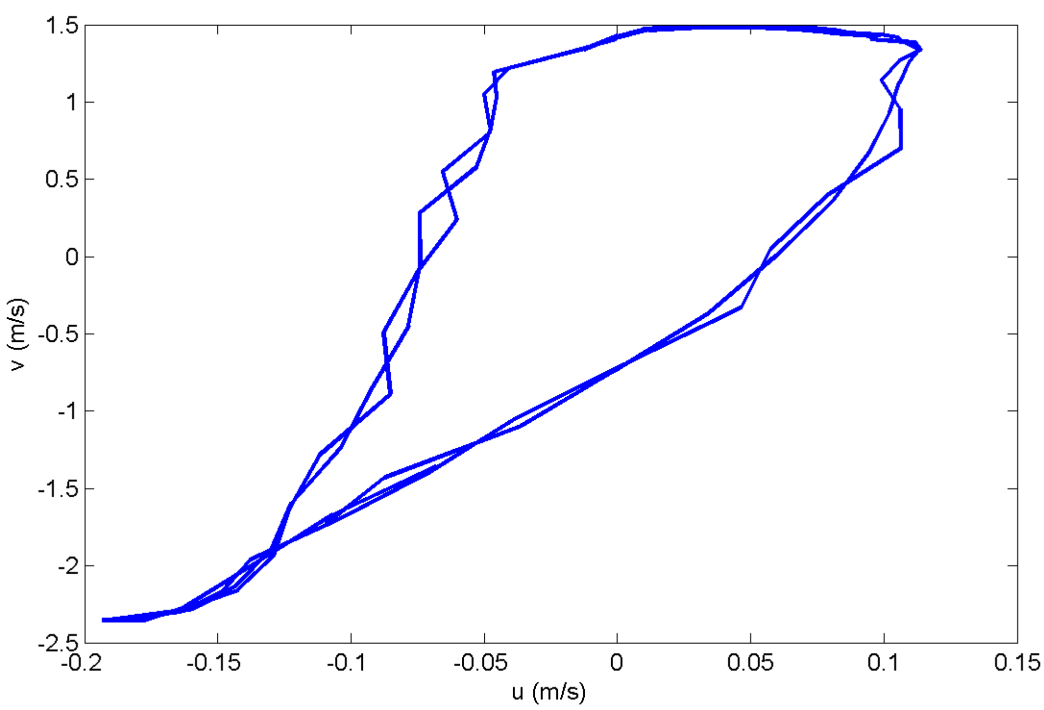

Fig. 11. Orbit of node no 3 (in a discretization grid of 100 nodes at *s*=41m from touch down) as seen from the side ($v=f(u)$), under heave excitation at the top with amplitude z_a=1.0m and circular frequency ω=1.5rad/s.

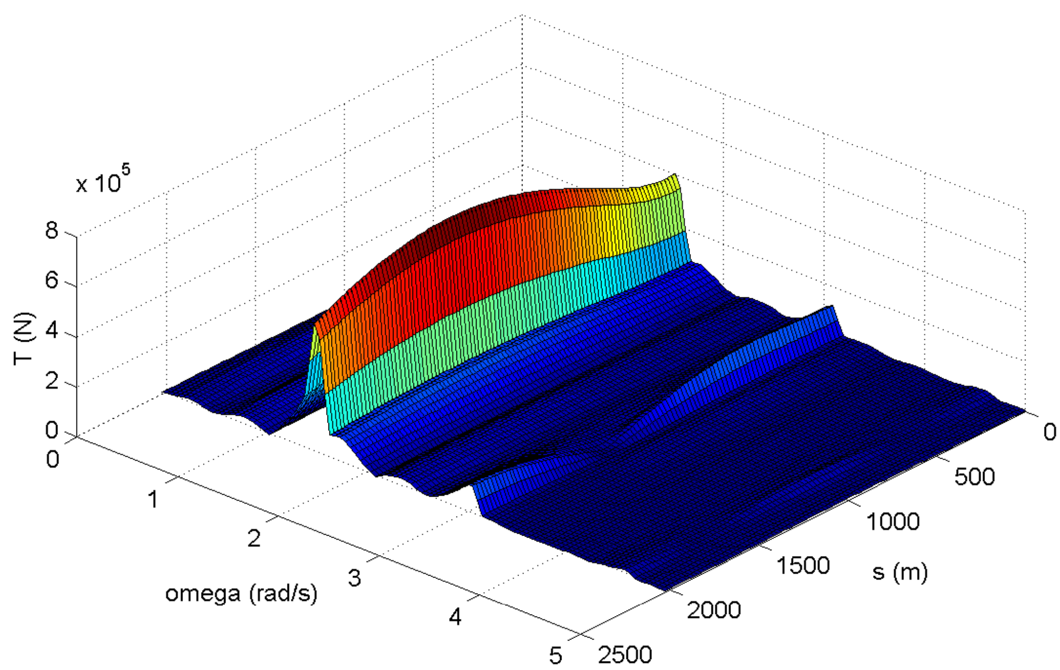

Fig. 12. Spectral densities of the dynamic tension T_1 along the catenary under heave excitation at the top, with amplitude z_a=1.0m and circular frequency ω=1.5rad/s.

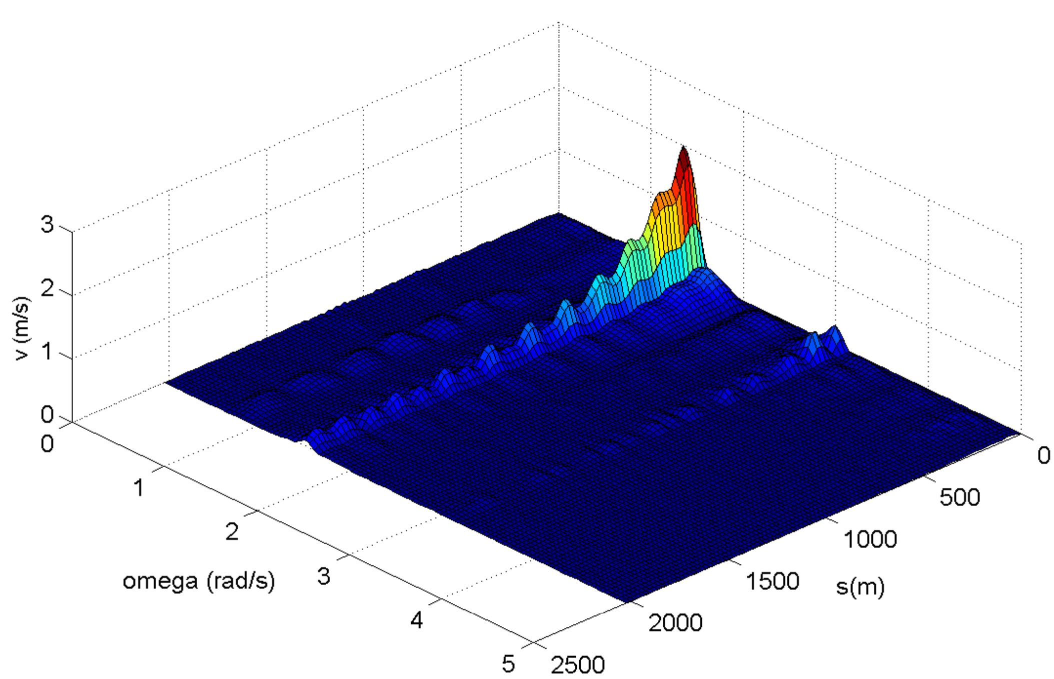

Fig. 13. Spectral densities of the normal velocity v along the catenary under heave excitation at the top, with amplitude z_a=1.0m and circular frequency ω=1.5rad/s.

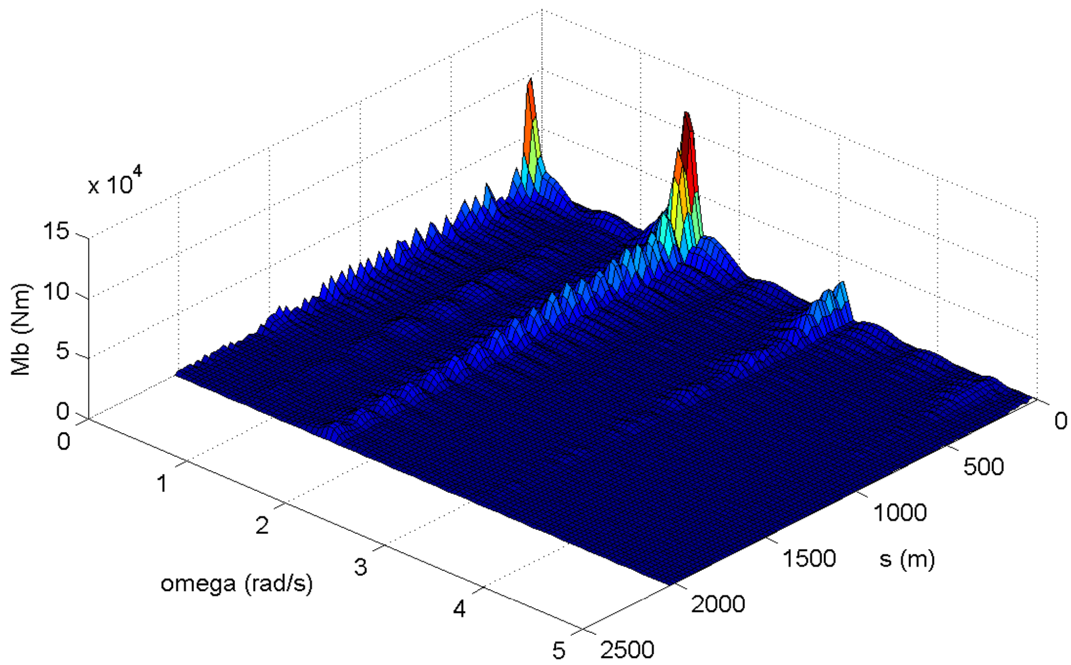

Fig. 14. Spectral densities of the in-plane dynamic bending moment M_{b1} along the catenary under heave excitation at the top, with amplitude z_a=1.0m and circular frequency ω=1.5rad/s.

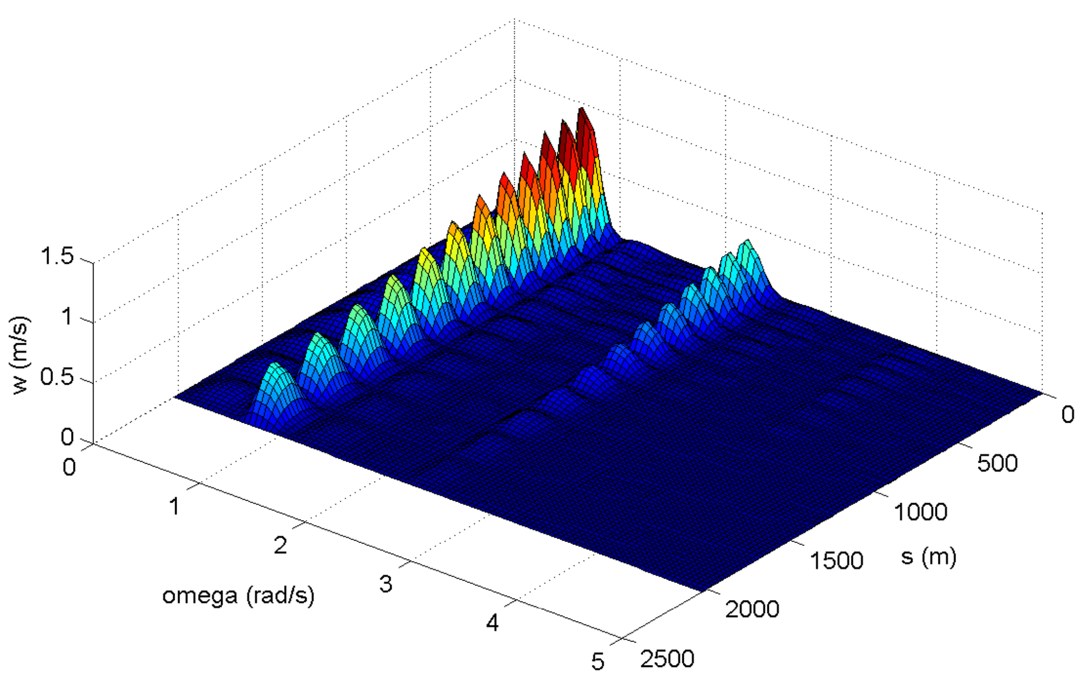

Fig. 15. Spectral densities of the bi-normal velocity w along the catenary under heave excitation at the top, with amplitude z_a=1.0m and circular frequency ω=1.5rad/s.

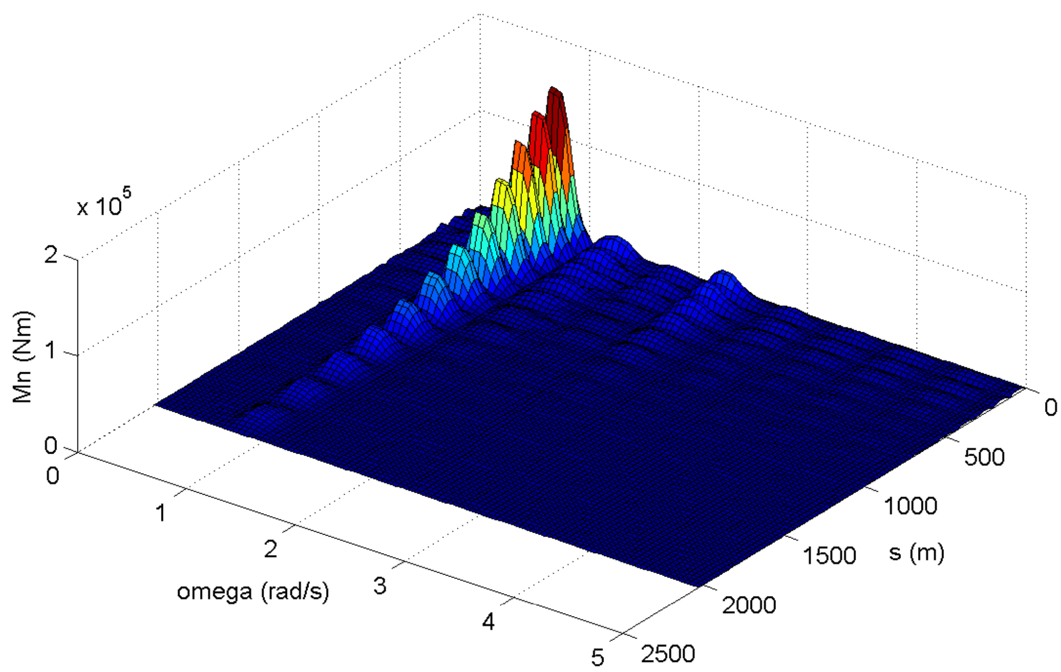

Fig. 16. Spectral densities of the out-of-plane dynamic bending moment M_{n1} along the catenary under heave excitation at the top, with amplitude z_a=1.0m and circular frequency ω=1.5rad/s.

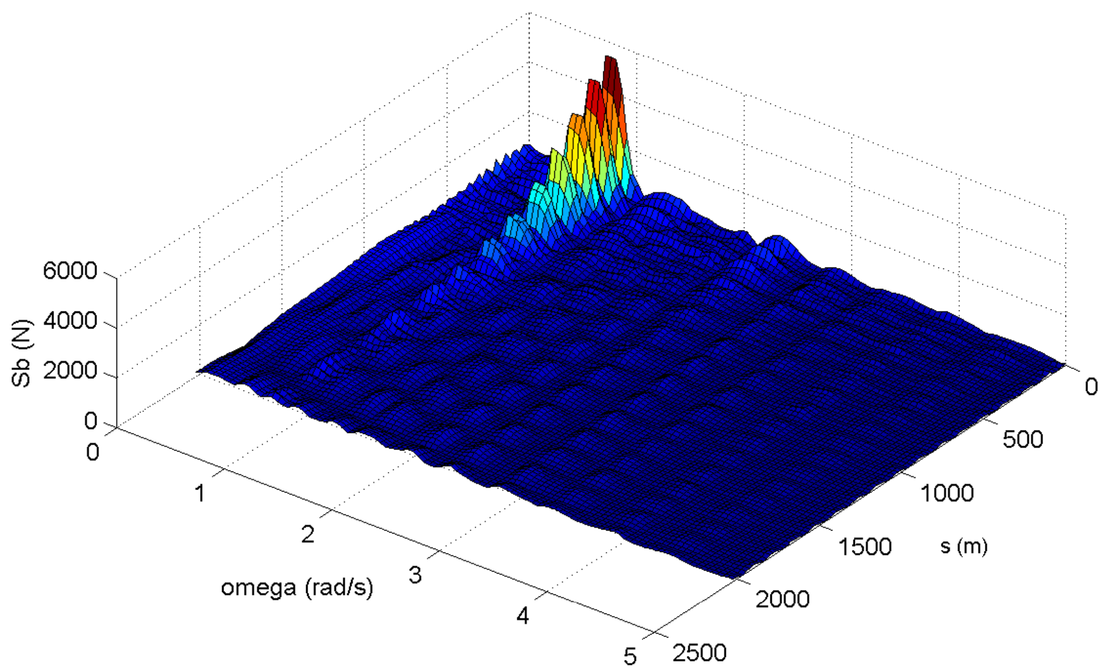

Fig. 17. Spectral densities of the out-of-plane dynamic shear force S_{b1} along the catenary under heave excitation at the top, with amplitude z_a=1.0m and circular frequency ω=1.5rad/s.

Nonlinear Dynamics
Edited by Todd Evans

ISBN 978-953-7619-61-9
Hard cover, 366 pages
Publisher InTech
Published online 01, January, 2010
Published in print edition January, 2010

This volume covers a diverse collection of topics dealing with some of the fundamental concepts and applications embodied in the study of nonlinear dynamics. Each of the 15 chapters contained in this compendium generally fit into one of five topical areas: physics applications, nonlinear oscillators, electrical and mechanical systems, biological and behavioral applications or random processes. The authors of these chapters have contributed a stimulating cross section of new results, which provide a fertile spectrum of ideas that will inspire both seasoned researches and students.